Nanostructures

DOI: 10.1002/anie.201103286

Capture of Radioactive Cesium and Iodide Ions from Water by Using Titanate Nanofibers and Nanotubes**

Dongjiang Yang, Sarina Sarina, Huaiyong Zhu, Hongwei Liu, Zhanfeng Zheng, Mengxia Xie, Suzanne V. Smith, and Sridhar Komarneni*

Radioactive Cs^+ and I^- ions are the products of uranium fission, and can be easily dissolved in water during an accident at a nuclear reactor, such as those that occurred at Chernobyl in 1986, at Three Mile Island in Pennsylvania in 1979, and in 2011 at Fukushima, Japan. In 2009, leaks of radioactive materials such as ^{137}Cs and ^{131}I isotopes also occurred during minor accidents at nuclear power stations in Britain, Germany, and the U.S. These leaks have raised concerns about exposure levels in the nearby communities because it is feared that these fission products could make their way into the food chain when present in waste water. Radioactive iodine is also used in the treatment of thyroid cancer, and, as a result, radioactive wastewater is discharged by a large number of medical research institutions.[1] The wide use of radioisotopes requires effective methods to manage radioactive waste, and methods currently used are complex and extremely costly.[2] Herein we demonstrate a potentially cost-effective method to remediate $^{137}Cs^+$ and $^{131}I^-$ ions from contaminated water by using the unique chemistry of titanate nanotubes and nanofibers, which can not only chemisorb these ions but efficiently trap them for safe disposal.

Inorganic cation exchangers, such as crystalline silicotitanates, zeolites, clay minerals, layered Zr phosphates, and layered sulfide frameworks, have been studied for separation of $^{137}Cs^+$ ions from nuclear wastewater and safe disposal of the exchanged cations because of the ability of these exchangers to withstand intense radiation and elevated temperatures, in addition to their high ion-exchange capacity.[3–9] Because ion exchange in materials is usually a reversible process, except in micas,[5] the radioactive ions in the exchanger may be released to water. Titanates are refractory mineral substances that are very stable with respect to radiation and chemical, thermal, and mechanical changes. Titanate nanofibers and nanotubes (with chemical formula $Na_2Ti_3O_7$) can be easily synthesized at low cost under hydrothermal conditions.[10] These materials possess a layered structure in which TiO_6 octahedra are the basic structural units (Figure S1 in the Supporting Information). These layers carry negative charges and are approximately two oxygen atoms thick.[10–13] Na^+ ions are situated between the layers and can be exchanged with other cations. In the present study, we show how trititanate nanofibers (T3NF) and nanotubes (T3NT) can be used to efficiently remove radioactive $^{137}Cs^+$ ions from aqueous solution by cation exchange.

Figure 1 a shows that the nanotubular T3NT can remove 80 % of $^{137}Cs^+$ ions from solutions with Cs^+ concentrations up to 250 ppm. The ions can be completely removed when the Cs^+ ion concentration is below 80 ppm. In contrast, the fibril T3NF has a comparatively lower absorption capacity than

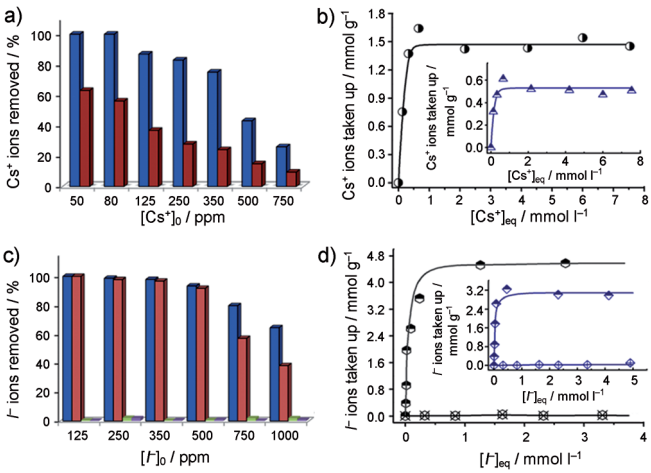

Figure 1. Removal of radioactive Cs^+ and I^- ions by sodium titanate nanotubes and nanofibers. Experimental details of the removal are provided in the Supporting Information. a) Removal of $^{137}Cs^+$ ions from solutions of different $^{137}Cs^+$ concentrations by the tubular T3NT (dark blue) and fibril T3NF (red) adsorbents. b) Isotherms for $^{137}Cs^+$ ion uptake by the titanate adsorbents. Circles: T3NT, triangles: T3NF. c) Removal of $^{125}I^-$ ions from solutions of different $^{125}I^-$ concentrations by titanates with anchored Ag_2O nanocrystals. Dark blue: Ag_2O-T3NT, red: Ag_2O-T3NF, green: T3NT, light blue: T3NF. d) Isotherms for $^{125}I^-$ adsorption by titanates with anchored Ag_2O nanocrystals. Filled circles: Ag_2O-T3NT, filled diamonds: Ag_2O-T3NF, empty diamonds: T3NF, empty circles: T3NT. For the above adsorption experiments, all of the data points represent the average of triplicate runs with a mean variation of less than ±3 %.

[*] Dr. D. Yang, S. Sarina, Prof. H. Zhu, Dr. H. Liu, Dr. Z. Zheng
Chemistry, Queensland University of Technology Institution
Brisbane, QLD 4001 (Australia)
E-mail: hy.zhu@qut.edu.au
Prof. M. Xie
Analytical & Testing Center, Beijing Normal University
Beijing 100875 (PR China)
Dr. S. V. Smith
Centre of Excellence in Antimatter Matter Studies
Australian Nuclear Science and Technology Organisation
Locked Bag 2001, Kirrawee DC NSW 2232 (Australia)
Prof. S. Komarneni
Materials Research Institute and
Department of Crop and Soil Sciences
The Pennsylvania State University, University Park, PA 16802 (USA)

[**] We gratefully acknowledge financial support from the ARC (DP0877108) and AINSE (ALNGRA10141P).

Supporting information for this article is available on the WWW under http://dx.doi.org/10.1002/anie.201103286.

T3NT. For instance, only around 36% of the $^{137}Cs^+$ ions were removed by the T3NF sorbent from solutions at a Cs^+ concentration of 125 ppm. The maximum capacity of T3NT for the uptake of $^{137}Cs^+$ ions was found to be approximately 1.5 mmol g^{-1}, while that of T3NF was substantially lower (ca. 0.5 mmol g^{-1}; Figure 1b). The large specific surface area (ca. 205 $m^2 g^{-1}$) of the nanotubes (ca. six times larger than that of the nanofibers; Table S1) is considered instrumental in the higher uptake ability of the nanotubes. An additional important characteristic of these materials is their rapid uptake. Both T3NT and T3NF reach maximum uptake within 10 min (Figure S2). It is noted that the adsorption capacity of the adsorbents decreases obviously when the pH value of the solution is lower than 3 (Figure S3A), because a large fraction of the Na^+ ions at the interlayers are exchanged with H^+ ions and thus the uptake of the Cs^+ ions is smaller. The adsorption of the nanofibers and nanotubes is not affected by high pH values as the materials were synthesized in 10 M NaOH solution, and are stable in highly basic solution. A large excess of competitive ions such as Na^+ ions in the solution slightly influence the Cs^+ adsorption of the titanates (Figure S3B).

TEM studies (Figure 2a) confirmed that the fibril morphology is maintained after uptake of Cs^+ ions. The sorbents can be easily separated from liquid suspensions after adsorption because of their fibril morphology.[14,15] Nonetheless, the uptake of a significant amount of Cs^+ ions can cause deformation of the titanate layers. From the electron diffraction patterns (EDP) in the [100] and [01$\bar{1}$0] directions (Figure 2d,e), apparent structural extinction was observed when l is odd; planes (00l) exhibit higher diffraction intensity when l is a multiple of four. The indexed results are shown in Figure 2f,g, and are consistent with the extinction rule of the hexatitanate nanofibers ($Na_2Ti_6O_{13}$, denoted as T6NF). T6NF fibers possess typical microporous tunnel structures and are usually obtained by heating T3NF fibers at 573 K.[15] The diffraction of the T3NF sample is clearly different from that of Cs-T3NF sample (a detailed analysis of the difference is provided in Figure S4 and S5). These results support the hypothesis that the uptake of large concentrations of Cs^+ ions can cause a phase transition from the initial layered structure of T3NF to T6NF to form microporous tunnels, in which the $^{137}Cs^+$ ions are entrapped. Such an important structural change was also verified by the XRD patterns (Figure 2c). Several diffraction peaks in the XRD patterns of T3NF disappeared because of the uptake of Cs^+ ions. The sample after the Cs^+ ion exchange (Cs-T3NF) possessed a d_{200} spacing of 0.778 nm, which is much less than the d_{100} spacing of T3NF (0.859 nm). Moreover, in the Raman spectra of the fibers before and after the exchange of Cs^+ ions (Figure S6), two typical peaks of T3NF at 309 cm^{-1} (vibration of the short Ti–O bond) and 883 cm^{-1} (vibration of the long Ti–O bond) disappear after exchange of $^{137}Cs^+$ ions. The absence of these peaks suggests that there is no terminal oxygen atom in corner-shared TiO_6 octahedron in the sample after $^{137}Cs^+$ ion exchange, as all the TiO_6 octahedra are corner-shared. This structure is characteristic of T6NF (see Figure 2h). This phase conversion is accompanied by the chemical reaction shown in Equation (1):

$$2\,Na_2Ti_3O_7 + (1-0.5x)\,Cs^+ + (1-0.5x)\,H^+ + H_2O \rightarrow Na_xCs_{1-0.5x}H_{1-0.5x}Ti_6O_{13} + (4-x)\,Na^+ + 2\,OH^- \quad (1)$$

The Cs^+ ions are located in the tunnels of the T6NF fibers.[15] The maximum width of the tunnel along the [010] direction is about 0.327 nm. Because the diameter of Cs^+ ion is 0.330 nm, it will be very difficult for the $^{137}Cs^+$ ions in the tunnels to diffuse and the ions are trapped in the fibers. T6NF is more stable than T3NF at higher temperatures; this property is an advantage for the safe disposal of the immobilized radioactive ions. The above-mentioned phase transition is different from that observed previously when titanate nanofibers were used to adsorb divalent radioactive radium and strontium cations.[14]

An intermediate [Cs-T3NF(i)] with lower Cs^+ ion content was prepared in a solution of CsCl with a lower concentration (3×10^{-4} M). The XRD pattern of this intermediate (Figure 2c) provides useful information on the structural transformation from T3NF to Cs-T3NF. The detailed analysis of the patterns supports the formation of a stable $Na_xCs_{1-0.5x}H_{1-0.5x}Ti_6O_{13}$ phase (see the Supporting Information). In this phase, the adjacent layers are linked by sharing the corner oxygen atoms, and the $^{137}Cs^+$ ions are entrapped in the tunnels. According to the elemental analysis data

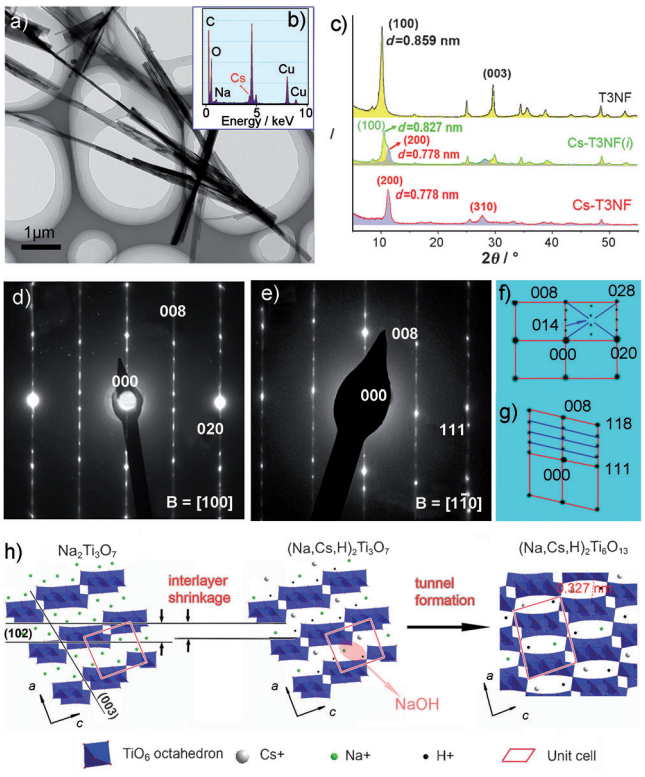

Figure 2. TEM micrograph, electron diffraction patterns (EDPs), and XRD patterns of titanate nanofibers after adsorption of Cs^+ ions. a) Low-magnification TEM image. b) Energy-dispersive X-ray spectrum (EDS) of the fibers in (a). c) XRD patterns of the nanofibers before and after exchange of Cs^+ ions. d,e) EDPs collected at [100] (d) and [01$\bar{1}$0] (e), and f,g) indexed results of the EDPs. h) Proposed structure evolution from layered T3NF to microporous tunnel T6NF caused by the exchange of Cs^+ ions.

obtained by EDS (Figure 2b), the atomic ratio of Na/Cs/Ti is 1.96:2.86:22.98. Assuming that the number of H^+ ions should be equal to that of Cs^+ ions in order to counteract the steric hindrance of the Cs^+ ions, the atomic ratio of (Na, Cs, H)/Ti is 1:2.99. This value is in agreement with the atomic ratio of Na/Ti (2:6) in T6NF.

In contrast, the Cs^+ ion uptake causes a serious morphological change of the titanate nanotubes (Figure S7). The pristine nanotubes have a diameter of approximately 8 nm, a length ranging from 100 to 200 nm, and an interlayer spacing of 0.72 nm. However, after Cs^+ ion uptake, the nanotubes (Cs-T3NT) become shorter (60–80 nm long) and thicker (with diameter ≈ 11 nm and interlayer spacing ≈ 0.85 nm, see Figure S7C,D). The elemental analysis data obtained by EDS (Figure S7E) shows that the atomic ratio of Na/Cs/Ti is 1.61:7.42:24.42. As the number of H^+ ions is equal to that of Cs^+ ions to counteract the steric hindrance effect of Cs^+ ions, the atomic ratio of (Na, Cs, H):Ti is 1:1.48, which is in good agreement with the atomic ratio of Na/Ti (2:3) in T3NT. Therefore, the layered structure of T3NT remained while the interlayer space expanded. The tubes consist of only a few layers and thus the interlayer space may swell to accommodate the large Cs^+ ions (Figure S8).

To capture and immobilize I^- ions from water, silver oxide (Ag_2O) nanocrystals with a size of 5–10 nm were anchored on external surfaces of T3NT or T3NF by dispersing them into an aqueous silver nitrate solution. In a neutral or basic suspension (pH ≥ 7) most of silver is in the form of Ag_2O nanoparticles (Ag_2O-T3NF, Figure 3a; Ag_2O-T3NT, Figure S9) and the remainder is in the form of Ag^+ ions in the interlayer region because of exchange with Na^+ ions. These Ag_2O nanoparticles efficiently capture I^- ions as the nanoparticles are exposed on the surface of the fibers or tubes and are thus readily accessible to the anions even in a fast flux. In the present study, because of a higher radiation dose of ^{131}I, we used stable $^{125}I^-$ ions together with radioactive I^- ions to monitor the behavior of the ^{131}I isotope. The two isotopes, however, have the same chemical reaction properties. Here the key issue is that the Ag_2O nanocrystals must be firmly attached to the titanate nanostructures. If the nanocrystals readily detach from the fibers or tubes, it will be extremely difficult and costly to recover the fine nanoparticles from a solution. Furthermore, the small Ag_2O nanocrystals may aggregate together to form a solid with low surface area and thus poor ability to precipitate I^- anions. Fortunately the Ag_2O crystals have surfaces of crystallographic similarity to the surface of the titanate nanostructures (Figure S10 of SI). The interplane distance of $(02\bar{1})_s$ planes of the Ag_2O crystals is 0.2102 nm, which is about one-quarter of the value for the $(50\bar{1})_t$ planes of the titanate (0.8396 nm), with a difference of about 0.1% (subscripts "t" and "s" denote the titanate phase and silver oxide phase, respectively). Another pair of matching planes is $(023)_t$ and $(200)_s$; the interplane distance of the $(100)_s$ planes, which is twice of that of the $(200)_s$ planes, is 0.4760 nm and about three times of that of the $(023)_t$ planes (0.1600 nm). When the Ag_2O nanocrystal and the titanate substrate join at these surfaces, the number of the oxygen atoms at the interface between the two phases, which are shared by the two phases, is maximized and full coordination

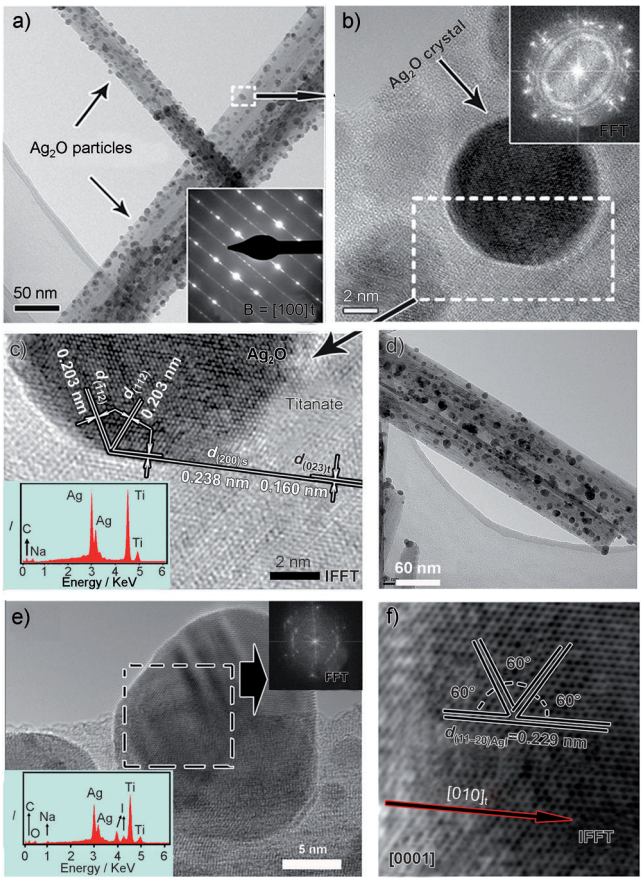

Figure 3. TEM images of the titanate nanofibers anchored with Ag_2O nanocrystals (Ag_2O-T3NF) and the titanate nanofibers coated with AgI nanocrystals (AgI-T3NF) formed by surface deposition of I^- ions. a) Typical TEM image showing the abundant Ag_2O crystals (5–10 nm) dispersed on titanate nanofibers. Inset: selected-area EDP of a single nanofiber. b) HRTEM image of an Ag_2O crystal. Inset: FFT image of the selected area. c) IFFT image of the selected area in (b). Inset: EDS spectrum of the composite nanofibers. d) TEM image of numerous AgI crystals (10–15 nm) formed on a single titanate nanofiber. e) HRTEM image of an AgI nanocrystal. Insets: FFT image of the selected area and the EDS of the AgI crystals on titanate nanofibers. f) IFFT image of the selected area in (e).

can be achieved to form well-matched phase interfaces (coherent interfaces). The Ag_2O nanocrystals are firmly anchored to the surface of the 1D titanate structures by such coherence interfaces. Figure 3b shows a high-resolution transmission electron microscopy (HRTEM) image of an Ag_2O nanocrystal on T3NF. Figure 3c shows the inverse fast fourier transition (IFFT) image of the selected area in Figure 3b; the lattice fringes can be clearly observed. As anticipated, the $(200)_s$ planes are parallel to the $(023)_t$ planes and the orientation $(02\bar{1})_s$ is parallel to $[100]_t$. Similarly, the Ag_2O crystals are anchored on the surface of titanate nanotubes by the coherent interface (Figure S9). Furthermore, the distribution of the Ag_2O nanocrystals can be readily controlled by adjusting the concentration of the Ag^+ ions in the aqueous silver nitrate solution (Figure S11).

As shown in Figure 1c, over 90% of $^{125}I^-$ ions at I^- ion concentrations below 500 ppm were removed by Ag_2O-T3NT.

Ag_2O-T3NF showed similar reaction properties. The reaction of $^{125}I^-$ ions onto pristine (without Ag_2O nanocrystals) T3NT and T3NF was less than 1% (Figure 1c). The capacities of the Ag_2O-T3NT and Ag_2O-T3NF sorbents for I^- ion sorption can be derived from the isotherms illustrated in Figure 1d. The approximate uptake capacity of the tubular Ag_2O-T3NT is 4.5 mmol of $^{125}I^-$ anions per gram of sorbent, while the capacity for the fibril Ag_2O-T3NF was slightly lower at 3.0 mmol g^{-1}. These uptake values are considerably higher than the values of less than 1.0 mmol g^{-1} previously reported for conventional metallic compound sorbents.[16]

Figure 3d shows the AgI nanocrystals are also firmly attached to the titanate nanofibers. The AgI crystals are slightly larger (10–15 nm, Figure 3e) than the parent Ag_2O crystals (5–10 nm). The TEM and HRTEM images of AgI crystals anchored on the nanotubes are shown in Figure S12. The EDS spectrum (Figure 3e), XRD patterns (Figure S13), and XPS spectra (Figure S14) indicate the presence of iodine in the used adsorbents.

It has been observed that the plane $(01\bar{1}0)$ of AgI crystal is parallel to [010] of the titanate fibers. Thus, the crystallographic registry between the two phases should be such that [0001] and $(01\bar{1}0)$ of the AgI crystal are parallel to [100] and (004) of the titanate fibers, respectively. Given that the interplanar distance of the $(01\bar{1}0)$ planes of AgI crystal is 0.2290 nm, which is close to that of the (004) planes of titanate nanofibers (0.2237 nm), the two planes can join together to form a well-matched interface between the two phases to bond the AgI crystals firmly to the titanate substrates (Figure S15).

To investigate the selective uptake of I^- ions by Ag_2O-NT and Ag_2O-NF adsorbents, we conducted the adsorption test in the presence of high concentrations of Cl^- ions (experimental details are given in the Supporting Information). Results of this experiment indicate that more than 99% of the I^- ions were taken up by either Ag_2O-NT or Ag_2O-NF in 0.1M NaCl solution. Clearly, the Ag_2O-T3NT and Ag_2O-T3NF were highly selective for I^- ions and the competing Cl^- ions had little effect on the I^- ion uptake capacity. The high selectivity should be ascribed to the large difference in the Gibbs energy of the reaction between Ag_2O and I^- or Cl^- ions (see the Experimental Section in the Supporting Information). The energy value is -32 kJ mol^{-1} for the reaction between Ag_2O and I^- and $+41$ kJ mol^{-1} for that between Ag_2O and Cl^-. Thus, the reaction between Ag_2O and NaI is much more favorable.

The structure evolution from the pristine titanate NF to Ag_2O-T3NF and the used sorbent are shown in Figure 4. Titanate NF consists of TiO_6 octahedral slabs, and the exposed plane is (100) (Figure 4a). When Ag^+ ions diffuse on the surface of titanate NF in a neutral or basic environment, silver hydrate intermediates, $Ag(OH)_n(H_2O)_m$, form on the surface. These intermediates will dehydrate with the surface Ti–OH and bond to the surface by sharing the surface oxygen atoms of the TiO_6 octahedron slabs in (100) planes (Figure 4b), thus resulting in the serious deformation of the surface (100) plane and thus the loss of diffraction intensity of this plane (Figure S13). In addition, the Ag^+ ions also exchanged with the Na^+ ions within the interlayer space,

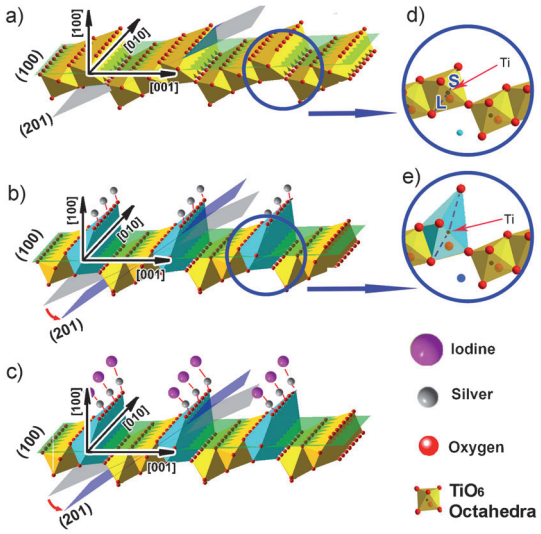

Figure 4. Profiles of Ag_2O nanocrystal formation on the (100) plane of the titanate nanofibers and the subsequent deposition of I^- ions (derived from the XRD patterns and Raman spectra). a) Surface of the titanate nanofibers. b,c) Deformation on (100) and (201) planes after the deposition of Ag_2O nanocrystals and subsequent I^- ion adsorption. d) Normal TiO_6 octahedron of the titanate substrates. e) Distorted TiO_6 octahedron showing that the very short Ti–O bond disappears and the very long Ti–O bond is elongated during deformation.

therefore resulting in the deterioration of crystallinity and decrease in diffraction intensity. The diffraction intensity of (201) planes (blue plane in Figure 4b) can be reduced substantially. The (201) planes are partially occupied by surface oxygen atoms and the Na^+ ions within the interlayer space in the pristine fibers. These Na^+ ions were replaced by the Ag^+ ions that have strong interactions with the oxygen atoms; this replacement can cause slight dislocation of the oxygen atoms from their original positions, which influences the diffraction intensity. The structure evolution was also verified by the variation of the short Ti–O bonds (the bonds between terminal oxygen atoms and the central titanium atom of the distorted TiO_6 octahedra, labeled S in Figure 4d) and the long Ti–O bonds (bonds between bridging oxygen atoms and the titanium atom in the same octahedron, labeled L in Figure 4d). Such variations were monitored by Raman spectroscopy (Figure S16).[17] Titanate NT has the same surface structure as the titanate NF, as NT formation can be regarded as scrolling multiple TiO_6 octahedral layers with a determined interlayer spacing.[18] A similar dehydration process of silver hydrate intermediates will take place on the outermost surface (100) planes. Hence, the diffraction peak of (100) planes disappears after the precipitation of Ag_2O nanocrystals (Figure S13). The iodide ions are captured by forming AgI crystals on the titanate surface. As shown in Figure 4c, the joint interface between the AgI nanocrystals and the titanate surface is composed of the silver atoms and the oxygen atoms of the Ti–O frameworks. Hence, the significant deformation caused by the precipitation of Ag_2O nanocrystals is still retained after deposition of I^- ions, as indicated by the XRD patterns (Figure S13).

Leaching or desorption of the precipitated $^{125}I^-$ ions was also tested (details of the experiment and results are given in the Supporting Information). The quantities of I^- ions released from the used samples into pure water or NaCl solutions are very low or below the detection limits. Evidently, with their superior adsorption properties, the Ag_2O-coated titanate sorbents are strong candidates for practical applications.

This study demonstrates that the unique structural properties of the titanate NTs and NFs make them superior materials for removal of radioactive Cs^+ and I^- ions in water. The 1D nanostructures of these materials provide a large external surface, which not only assures a high capacity for the uptake of cations and anions and very fast kinetics, but also facile separation of the adsorbents from solutions for ultimate safe disposal. Finally, these fibers and tubes can be fabricated readily from TiO_2 at low cost.[10] The ability to tailor these structural features to enhance uptake and trapping of ions can be exploited for further development of new and selective adsorbents for the removal of other toxic cations and anions that may be found in groundwater or wastewater.

Received: May 13, 2011
Revised: August 9, 2011
Published online: September 20, 2011

Keywords: cesium · iodine · nanostructures · radioactive ions · titanates

[1] J. E. Martin, F. D. Fenner, *Public Health Rep.* **1997**, *112*, 308–318.
[2] A. L. Mascarelli, *Nature* **2009**, *458*, 1086–1087.
[3] a) A. J. Celestian, J. D. Kubicki, J. Hanson, A. Clearfield, J. B. Parise, *J. Am. Chem. Soc.* **2008**, *130*, 11689–11694; b) A. J. Celestian, J. B. Parise, R. I. Smith, B. H. Toby, A. Clearfield, *Inorg. Chem.* **2007**, *46*, 1081–1089; c) P. Sylvester, A. Clearfield, *Solv. Extr. Ion Exch.* **1998**, *16*, 1527–1539; d) K. A. Venkatesan, V. Sukumaran, M. P. Antony, T. G. Srinivasan, *J. Radioanal. Nucl. Chem.* **2009**, *280*, 129–136; e) E. A. Behrens, P. Sylvester, A. Clearfield, *Environ. Sci. Technol.* **1998**, *32*, 101–107.
[4] S. Komarneni, R. Roy, *Science* **1988**, *239*, 1286–1288.
[5] S. Komarneni, R. Roy, *Nature* **1982**, *299*, 707–708.
[6] A. Dyer, M. Pillinger, S. Amin, *J. Mater. Chem.* **1999**, *9*, 2481–2487.
[7] L. R. Van Loon, B. Baeyens, M. H. Bradbury, *Appl. Geochem.* **2009**, *24*, 999–1004.
[8] N. Ding, M. G. Kanatzidis, *Nat. Chem.* **2010**, *2*, 187–191.
[9] A. Clearfield, *Nat. Chem.* **2010**, *2*, 161.
[10] H. Y. Zhu, Y. Lan, X. P. Gao, S. P. Ringer, Z. F. Zheng, D. Y. Song, J. C. Zhao, *J. Am. Chem. Soc.* **2005**, *127*, 6370–6376.
[11] Y. I. Kim, S. Salim, M. Huq, T. E. Mallouk, *J. Am. Chem. Soc.* **1991**, *113*, 9561–9563.
[12] N. Sukpirom, M. M. Lerner, *Chem. Mater.* **2001**, *13*, 2179–2185.
[13] S. Andersson, A. D. Wadsley, *Acta Crystallogr.* **1962**, *15*, 194–201.
[14] D. Yang, Z. Zheng, H. Zhu, H. Liu, X. Gao, *Adv. Mater.* **2008**, *20*, 2777–2781.
[15] D. Yang, Z. Zheng, H. Liu, E. R. Waclawik, X. Ke, M. Xie, H. Zhu, *Phys. Chem. Chem. Phys.* **2010**, *12*, 1271–1277.
[16] G. Lefèvre, A. Walcarius, J.-J. Ehrhardt, J. Bessire, *Langmuir* **2000**, *16*, 4519–4527.
[17] S. Papp, L. Korosi, V. Meynen, P. Cool, E. F. Vansant, I. Dekany, *J. Solid State Chem.* **2005**, *178*, 1614–1619.
[18] Q. Chen, G. H. Du, S. Zhang, L.-M. Peng, *Acta Crystallogr. Sect. B* **2002**, *58*, 587–593.

